Dalton Transactions

ROYAL SOCIETY OF CHEMISTRY

PAPER

View Article Online
View Journal

Cite this: DOI: 10.1039/d5dt02262b

Structural investigation of the protonation states of sulfamic acid

Valentin Bockmair, *[a] Andreas Klöck, [a] Lukas Stanzel,[a] Sven Ringelband,[b] Frank Tambornino [b] and Andreas J. Kornath†[a]

Received 21st September 2025,
Accepted 30th October 2025

DOI: 10.1039/d5dt02262b

rsc.li/dalton

Herein, we report on the *O*-monoprotonated and double *O*-hemiprotonated species of sulfamic acid in the binary superacidic systems HF/L (L = BF_3, GeF_4, AsF_5, SbF_5). Within the structural studies, differences in the coordination behavior of the weakly coordinating anions MF_6^- (M = As, Sb) were determined. The colorless salts were characterized by low-temperature vibrational spectroscopy and single-crystal X-ray diffraction. The experimental data are discussed together with quantum chemical calculations in the solid state at the DFT-TZVP/PBE0-(D3) level of theory. Furthermore, the decomposition of sulfamic acid in basic milieu was investigated.

Introduction

Sulfamic acid, also known as amidosulfuric acid (ASA), has diverse applications both in everyday life and in science. ASA is produced on a ton scale due to the unique properties as an effective descaling agent,[1] as well as for the refinement of metals.[2] ASA is generally synthesized by reacting urea with oleum (see. Scheme 1).[3–7] Neutron diffraction experiments on single crystals revealed the zwitterionic character in the molecular structure of ASA (see Scheme 1),[8] similar to glycine and its organic aminoalkylsulfonic acid derivatives aminomethanesulfonic acid or aminoethansulfonic acid (taurine).[9,10]

Strong acids are defined by negative pK_a values, ASA with a pK_a value of 1, is not a strong acid.[11] Investigations carried out by Hopfinger in 2012 postulated that the monoprotonated ammoniumsulfonic acid hexafluoridometallate can be obtained in the binary superacidic system HF/MF_5 (M = Sb, As) at −50 °C (see Scheme 2).

This would be in good accordance with earlier investigation of the protonation of taurine carried out by Hopfinger. Its protonation led to the formation of the corresponding ammoniumethylsulfonic acid hexafluoridostibate salt (see Scheme 3).[12] As shown by our working group, the reported Raman spectrum contained lines attributable to the diprotonated species of taurine, containing a sulfonium ($-SO_3H_2^+$) moiety (see Scheme 3).[13]

The rise of temperature seemed to allow for higher degrees of protonation if enough Lewis acid was provided.

However, a closer examination of the vibrational data reveals that some of the values of the observed modes differ significantly from the calculated values. This led us to question whether a higher degree of protonation might be present for ASA, such as it is the case for taurine. Upon protonation of ASA, the stability of the expected ammoniumsulfonium dication might suffer from intramolecular repulsion, as representing a vicinal superelectrophile.

Since no single crystals of the monoprotonated species of ASA were obtained before, it can only be assumed that the determination of the degree of protonation solely through

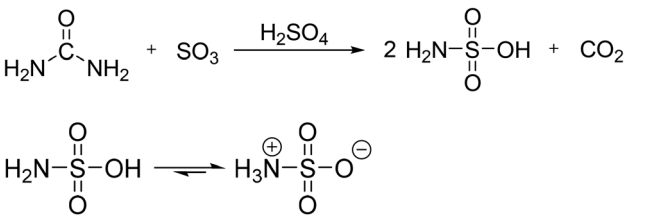

Scheme 1 Industrial synthesis of ASA (top) and tautomerism of the ASA zwitterion (bottom).

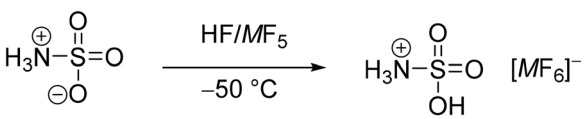

Scheme 2 Protonation of ASA in the binary superacidic media (M = As, Sb).

[a]Chair of Inorganic Chemistry, Department of Chemistry, University of Munich (LMU), 81377 Munich, Germany. E-mail: valentin.bockmair@cup.uni-muenchen.de
[b]Chair of Inorganic Chemistry, Department of Chemistry, Philipps University, Marburg, Germany
† Deceased

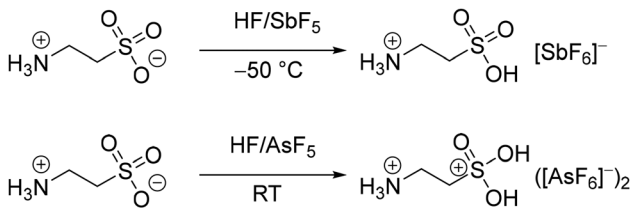

Scheme 3 Taurine in the binary superacidic media at low temperature (top) and room temperature (bottom).

vibrational spectroscopy is very challenging.[14] Therefore, investigations of ASA in the binary superacidic systems HF/L (L = BF_3, GeF_4, AsF_5, SbF_5) were carried out at room temperature.

Furthermore, we investigated the reaction with bases based on previous titration experiments, indicating that the zwitterion could be deprotonated analogously to aminomethanesulfonic acid with copper carbonate.[15]

Results and discussion

Protonation of ASA

Similar to the protonation of aminomethanesulfonic acid, anhydrous hydrogen fluoride is not acidic enough to protonate ASA (see Scheme 4). By the addition of a Lewis acid, such as BF_3, GeF_4, AsF_5 or SbF_5, protonation occurs on the *O*-site of the zwitterion, leading to the formation of the ammonium sulfonic acid salt (see Scheme 4). As identified by single crystal structure analysis, all obtained salts are monoprotonated, which is in contrast to aminoalkylsulfonic acids, such as aminomethanesulfonic acid and taurine (see Scheme 4). Even by providing stronger Lewis acids, MF_5 (M = As, Sb) no further protonation could be observed up to room temperature.

While rather strong coordinating anions $[BF_4]^-$ and *cis*-$[GeF_5]^-$ (*cis*-bridged polymeric) tend to form classical monoprotonated species, the salts containing the weakly coordinating anions $[MF_6]^-$ (M = As (**4**), Sb (**5**)) crystallize as twofold hemi-protonated species.

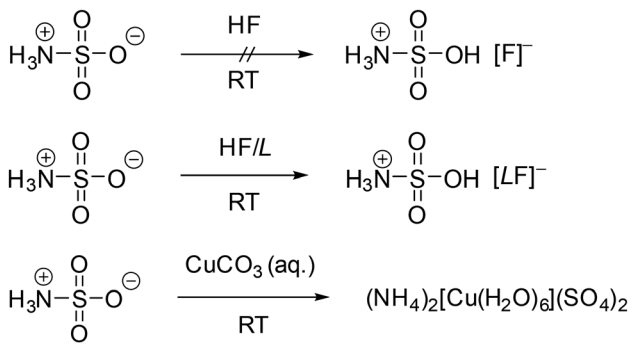

Scheme 4 ASA in anhydrous HF (top), protonation of ASA in binary superacidic media (L = BF_3, GeF_4, AsF_5, or SbF_5) (middle) and decomposition reaction of ASA with $CuCO_3$ (bottom).

Deprotonation of ASA

Attempting to deprotonate ASA with copper(II) carbonate, led to decomposition, detected by the formation of $(NH_4)_2[Cu(H_2O)_6](SO_4)_2$, as identified by single crystal X-ray analysis (see Scheme 4).[16]

In contrast to the reaction with the copper(II) carbonate, treatment of ASA with aqueous amines (methylamine, dimethylamine, and triethylamine) shows no visible conversion, as the evaporation of the reaction mixture only led to recrystallization of ASA.

Crystal structures

The donor–acceptor interactions of the molecular unit and cationic units are illustrated in Table 1–4. Bond lengths of the starting material and protonated species are compared in Table 5. The strength of hydrogen bonding was classified according to Jeffrey.[17]

Crystal structure of ASA (1)

ASA crystallizes in the orthorhombic space group *Pbca* with eight formula units per unit cell and one molecule in the asymmetric unit.

The S–N (1.759(1) Å) and S=/–O (1.429(1) Å, 1.431(1) Å, and 1.434(1) Å) bond lengths are in good accordance with structurally related compounds (see Table 5).[18]

The zwitterions in the crystal structure of ASA are linked by 12 medium to weak hydrogen bonding interactions (2.768(2)–2.943(2) Å; see Table 1 and Fig. 1). Furthermore, due to the distance of O3···O1 3.026(2) Å, two weak orbital interaction can be suggested ($n_{(O1)} \rightarrow \sigma^*_{(O3-S1)}$).

Crystal structure of [ASA + 1H][BF_4]·ASA (2)

The tetrafluoroborate salt of amido sulfuric acid crystallizes together with ASA in the monoclinic space group $P2_1/n$. The asymmetric unit consists of one $[BF_4]^-$ anion, one ammoniumsulfonic acid cation, and one cocrystallized molecule of amido sulfuric acid (see Fig. 2). The unit cell comprises four formula units.

Whereas the S–N bond lengths (1.766(2) Å and 1.764(2) Å) are nearly unaffected by the protonation (within 3σ), the S=/–O bond lengths differ significantly from the starting material. Due to the mesomeric delocalization of S=O double bonds in the zwitterion of ASA, all SO bond lengths are nearly equal. Upon protonation, the S1–O1 bond length (1.507(2) Å) is sig-

Table 1 Selected donor–acceptor distances of ASA (**1**) in [Å]

O2···(H1i)N1i	2.768(2)	O2···(H2i)N1i	2.768(2)
O3···(H1i)N1i	2.900(2)	O3···(H3i)N1i	2.900(2)
O1···(H2iii)N1iii	2.904(2)	O1···(H3iii)N1iii	2.904(2)
O3···(H2ii)N1ii	2.917(2)	O3ii···(H2)N1	2.917(2)
O2···(H3iii)N1iii	2.941(2)	O2iii···(H3)N1	2.941(2)
O1···(H1iii)N1iii	2.943(2)	O1iii···(H1)N1	2.943(2)
O3i···O1	3.026(2)	O3···O1i	3.026(2)

Symmetry codes: i = screw axis 2-fold (along [0,0,1], [0,1,0] and [1,0,0]); ii = –x,–y, –z; iii = glide plane (along [0,0,1], [0,1,0] and [1,0,0]).

Table 2 Interatomic distance of the [ASA + 1H]$^+$ cation (top) and ASA (below) in the crystal structure of [ASA + 1H][BF_4]·ASA (**2**) in [Å]

O4···(H1)O1	2.495(2)	O3···(H2Bi)N2i	2.898(2)
O6ii···(H1A)N1	2.787(2)	O3···(H2Ci)N2i	2.898(2)
F1···(H1C)N1	2.846(2)	F2···(H1C)N1	2.906(2)
F1···(H1B)N1	2.846(2)	F4ii···(H1B)N1	2.936(2)
F1ii···(H1B)N1	2.867(2)	O1i···S1	3.283(2)
O2···(H1B)N1	2.878(2)	O1···S1i	3.283(2)
O2···(H1B)N1	2.878(2)		
O4···(H1)O1	2.495(2)	F3ii···(H2A)N2	2.844(2)
O5···(H2B)N2	2.709(3)	F4iii···(H2A)N2	2.853(2)
O5···(H2B)N2	2.709(3)	O3i···(H2B)N2	2.898(2)
O6···(H2Bii)N1ii	2.787(2)	O3i···(H2C)N2	2.898(2)

Symmetry codes: i = 1/2 − *x*, 1/2 + *y*, 1/2 − *z*; ii = −*x*,−*y*,−*z*; iii = 1/2 + *x*, 1/2 − *y*, 1/2 + *z*.

Table 3 Interatomic distance of the [ASA + 1H]$^+$ cation in [ASA + 1H][GeF_5] (**3**) in [Å]

F1···(H1)O1	2.460(3)	F3i···(H1B)N1	2.804(3)
O3···(H1Ai)N1i	2.712(4)	O2···(H1C)N1	2.834(4)
O3···(H1Bi)N1i	2.712(4)	O2···(H1C)N1	2.834(4)
O3···(H1Ci)N1i	2.712(4)	F3i···(H1B)N1	2.840(3)
O3i···(H1A)N1	2.712(4)	F2i···O2	2.974(3)
O3i···(H1B)N1	2.712(4)	F1i···O1	2.978(3)
O3i···(H1C)N1	2.712(4)	F3i···(H1C)N1	3.138(3)
F4i···(H1A)N1	2.750(3)		

Symmetry codes: i = −1/2 − *x*,−*y*, 1/2 + *z*,−*x*, 1/2 + *y*, 1/2 − *z*; 1/2 + *x*, 1/2 − *y*,−*z* (screw axis (2-fold)).

Table 4 Interatomic distance of [ASA + 1H][SbF_6] (**5**) in [Å]

O2(H2)···O2i	2.688(4)	F5···(H1B)N1	2.927(4)
O1(H1)···O1i	2.781(5)	F5···(H2)O2	2.959(3)
F1···(H1)O1	2.883(4)	O3···(H1B)N1	3.023(4)
F2···(H1C)N1	2.902(4)	O3···(H1B)N1	3.023(4)
F6···(H1C)N1	2.906(4)	F2i···(H1C)N1	3.065(3)
F4i···(H1A)N1	2.908(4)	F4i···(H1B)N1	3.080(3)
F3···(H1A)N1	2.924(4)	F3i···(H1A)N1	3.115(3)

Symmetry codes: i = −*x*,−*y*,−*z*.

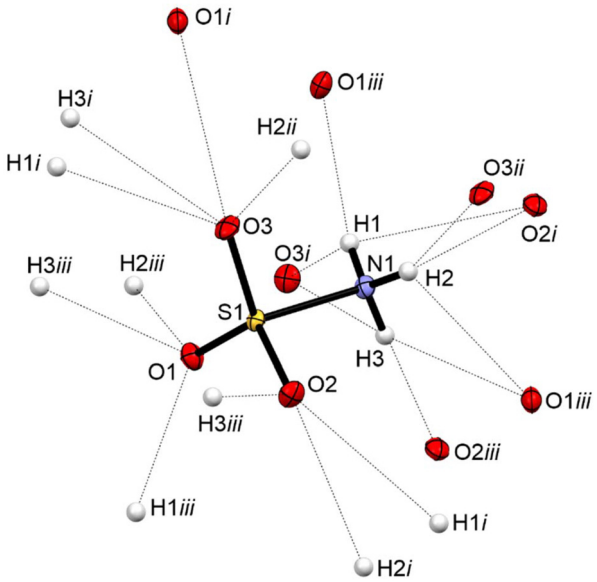

Fig. 1 Short contacts of the asymmetric unit of ASA (displacement ellipsoids drawn with 50% probability).

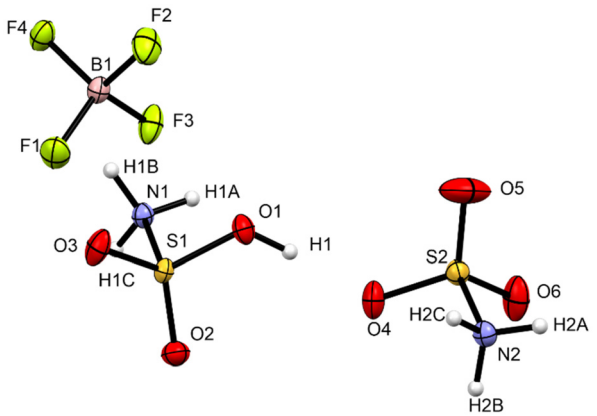

Fig. 2 Asymmetric unit of [ASA + 1H][BF_4]·ASA (**2**), viewed along the *c* axis (displacement ellipsoids drawn with 50% probability).

nificantly elongated, accompanied by shortening of the terminal S–O bond lengths (1.414(2) Å and 1.410(2) Å). As the SO bond lengths (1.449(2) Å,1.424(2) Å, and 1.414(2) Å) in the cocrystallized ASA molecule of (**2**) only deviate weakly from the values in the starting material and are involved in a stronger hydrogen bond network, this can be referred to packing effects, rather than hemi-protonation of ASA.

In contrast to the cocrystallized ASA molecule, the number of interatomic donor–acceptor interactions are increased in the [ASA + 1H]$^+$ cation (see Fig. 3). Both molecules show one strong hydrogen bond and medium to weak interactions (see Table 2). Furthermore, weak $n_{(O1)} \rightarrow \sigma^*_{(S1-N1)}$ can be detected in the crystal structure of the $[BF_4]^-$ salt, at the distance of 3.283(2) Å.

The tetrafluoroborate anion shows the expected B–F bond lengths (1.384(3)–1.407(3) Å) comparable values to from literature.[19,20]

Table 5 Bond length comparison of ASA and protonated species (**2**,**3**,**5**) in [Å]

ASA (**1**)		ASA (**2**)		[ASA + 1H]$^+$ (**2**)		[ASA + 1H]$^+$ (**3**)		[ASA + 1H]$^+$ (**5**)	
S1–O1	1.429(1)	S2–O4	1.449(2)	S1–O1	1.507(2)	S1–O1	1.505(3)	S1–O2	1.454(3)
S1–O2	1.431(1)	S2–O6	1.424(2)	S1═O3	1.414(2)	S1═O2	1.416(3)	S1–O1	1.450(4)
S1–O3	1.434(1)	S2–O5	1.414(2)	S1═O2	1.410(2)	S1═O3	1.412(3)	S1═O3	1.409(3)
S1–N1	1.759(1)	S2–N2	1.766(2)	S1–N1	1.764(2)	S1–N1	1.736(3)	S1–N1	1.765(3)

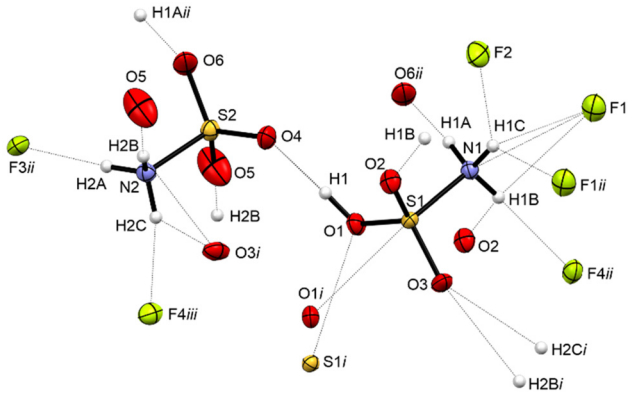

Fig. 3 Short contacts of [ASA + 1H][BF_4]·ASA (displacement ellipsoids drawn with 50% probability). Symmetry codes: i = 1/2 − *x*, 1/2 + *y*, 1/2 − *z*; ii = −*x*,−*y*,−*z*; iii = 1/2 + *x*, 1/2 − *y*, 1/2 + *z*.

Crystal structure of [ASA + 1H][GeF_5] (3)

The *cis*-[GeF_5]$^-$ salt of protonated ASA crystallizes in the non-centrosymmetric orthorhombic space group $P2_12_12_1$ with four formula units per cell. The asymmetric unit comprises one [ASA + 1H]$^+$ cation and one [GeF_5]$^-$ unit (see Fig. 4).

In contrast to the [BF_4]$^-$ salt **2**, the [GeF_5]$^-$ salt **3** forms a single classical monoprotonated cationic species. The S=/–O bond lengths (1.505(3) Å, 1.416(3) Å, and 1.412(3) Å) in the [ASA + 1H]$^+$ (**3**) cation are in good accordance with those of **2**, the S–N bond length is significantly shortened to 1.736(3) Å (see Table 5), with respect to the 3σ rule.

The Ge–F bond lengths (1.731(2)–1.889(2) Å) are comparable to other literature known [GeF_5]$^-$ salts.[21,22]

Similar to the monoprotonated species in **2**, the [ASA + 1H]$^+$ cation forms one strong and 11 medium to weak hydrogen bonds (see Table 3 and Fig. 5).

The anions built up a planar network of isolated *cis*-$^1_\infty$[GeF_5]$^-$chains. These chains are intercalated into hydrogen-bond-dominated lattices of monoprotonated ASA (see Fig. 6).

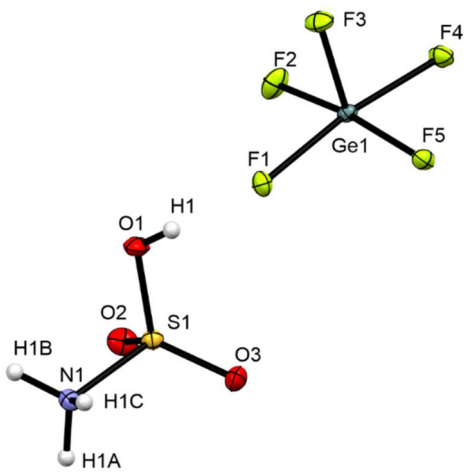

Fig. 4 Asymmetric unit of [ASA + 1H][GeF_5] (**3**), viewed along the *a* axis (displacement ellipsoids drawn with 50% probability).

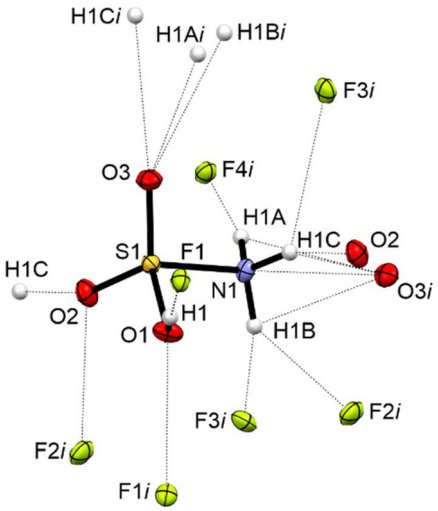

Fig. 5 Short contacts of [ASA + 1H][GeF_5] (**3**) (displacement ellipsoids drawn with 50% probability). Symmetry codes: i = −1/2 − *x*,−*y*, 1/2 + *z*,−*x*, 1/2 + *y*, 1/2 − *z* and 1/2 + *x*, 1/2 − *y*,−*z* (screw axis (2-fold)).

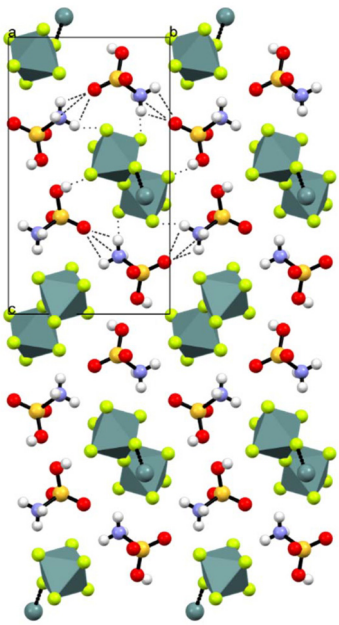

Fig. 6 Polyhedral illustration of the slicing of [ASA + 1H][GeF_5] (**3**), viewed along the *a* axis and hydrogen bonding network around the unidirectional chains of [GeF_5]$^-$ anions.

Crystal structure of [ASA + 1H][MF_6] (M = As (4), Sb (5))

The investigated [MF_6]$^-$ salts of twofold hemi-protonated ASA crystallize isostructurally in the triclinic space group $P\bar{1}$ with two formula units per unit cell and half-occupied positions of H1 and H2 (see Fig. 7). Twofold hemi-protonated species are especially found in planar cations, allowing chains of cations; therefore, the appearance in the 3D structure is rather uncommon.[23,24]

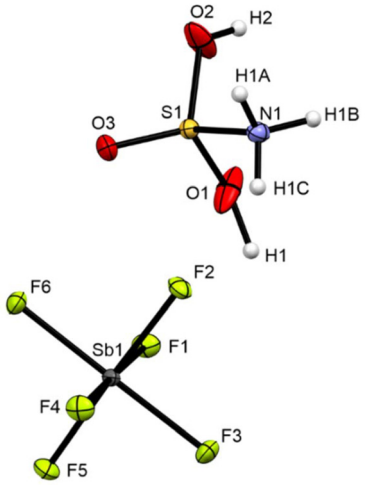

Fig. 7 Asymmetric unit of [ASA + 1H][SbF_6] (**5**), viewed along the *a* axis (displacement ellipsoids drawn with 50% probability; half-occupation of H1 and H2).

The S═/–O bond lengths (1.454(3) Å, 1.450(4) Å, and 1.409 (3) Å) follow the trend of the monoprotonated species, but the elongation of the S═/–O bond length upon protonation is distributed across both hemi-protonated sites. Furthermore, the remaining S═O bond is shortened, similar to **2** and **3**. The SN bond length (1.765(3) Å) observed in the cation is equal to that in **2**.

In Fig. 8, the short contacts of the twofold hemi-protonated species of ASA are depicted. The strongest hydrogen bonds are found between the hemi-protonated sites at the distance of 2.688(4) and 2.781(5) Å. Furthermore, two hydrogen bonds are formed with the twofold hemi-protonated sites and with the anion at the distance of 2.883(4) Å and 2.959(3) Å. Ten weaker interactions are observed between the ammonium moiety and the sulfuryl oxygen or fluoride acceptors atoms of the anions of as detected to a distance of 2.902(4)–3.115(3) Å (see Table 4).

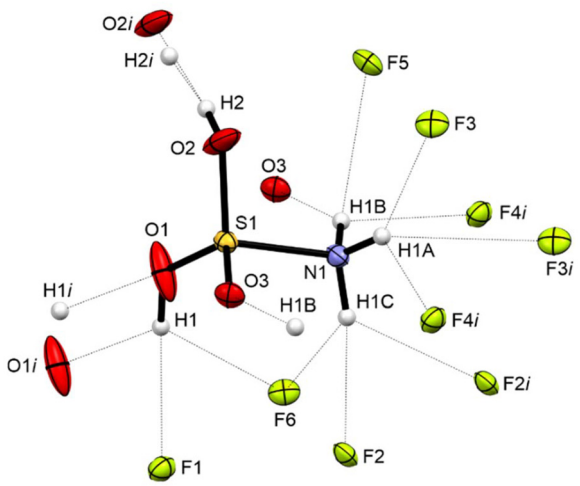

Fig. 8 Short contacts of the asymmetric unit of [ASA + 1H][SbF_6] (displacement ellipsoids drawn with 50% probability). Symmetry codes: i = –*x*,–*y*,–*z*.

Hirshfeld surface analysis (see Fig. 9) of the starting material, **3** and **5**, is depicted in Fig. 9. It emphasizes the numerous contacts, and the difference in the contact behaviour of **3** (strongly coordinating) and **4**,**5** (weakly coordinating).

Vibrational spectroscopy

The low-temperature Raman spectra of ASA (**1**) and its protonated species [ASA + 1H][BF_4] ·ASA (**2**), [ASA + 1H][GeF_5] (**3**), [ASA + 1H][AsF_6] (**4**), and [ASA + 1H][SbF_6] (**5**) are illustrated in Fig. 10.

In Tables S21–24, selected observed vibrational frequencies of **1**–**5** are listed together with the quantum chemically calculated frequencies of the solid-state structures containing the $[ASA + 1H]^+$ cation as well as their assignments. The ASA zwitterion in the crystal structure has 18 fundamental modes and processes C_{3v} symmetry. The assignment is shown in Table S21.

As already mentioned in the literature,[25] the calculation of vibrational spectra of zwitterionic structures deviates in parts from observed experimental values. Especially, the calculated ν(N–H) stretching vibrations are shifted to higher wavenumbers compared to the observed values, whereas the $\nu(SO_3)$ and the ν(N–S) vibrational frequencies are in good accordance with calculated data.

The $[ASA + 1H]^+$ cation in the crystal structure has 21 fundamental modes of and possesses C_1 symmetry. The assignments are shown in Table S22–24 for (**2**–**5**).

The monoprotonated species of ASA, [ASA + 1H][GeF_5] shows the expected shifts as calculated, with the exception of the splitting of some modes. Compared with the starting material, the ν(N–S) stretching mode is shifted to higher wavenumbers due to the strengthening effect upon protonation, similar as observed upon protonation of organosulfonic acids.[26] The vibrational spectroscopic data of the anions are in good accordance with the literature-known frequencies.[22] The twofold hemi-protonated species **4** and **5** show similar frequencies due to the amount of Lewis acid used, the spectra of **5** also show the coexistence of the $[Sb_2F_{11}]^-$ salt beside the crystallized $[SbF_6]^-$ salt. Furthermore, the Raman lines in the spectra of **4** benefit from better visibility as the lines of the $[AsF_6]^-$ (O_h) salt are smaller. Due to the distribution of the protonated sites, the ν(N–S) is only shifted marginally compared to the starting material. Beyond that, the experimental and the calculated are nearly equal, as expected for isostructural compounds.

The vibrational spectroscopic data of the anions are in good accordance with the literature-known frequencies.[12,13,22]

Theoretical calculations

The structure optimization of ASA (**1**), [ASA + 1H][BF_4]·ASA (**2**), [ASA + 1H][GeF_5] (**3**) and [ASA + 1H][MF_6] (**4**,**5**)

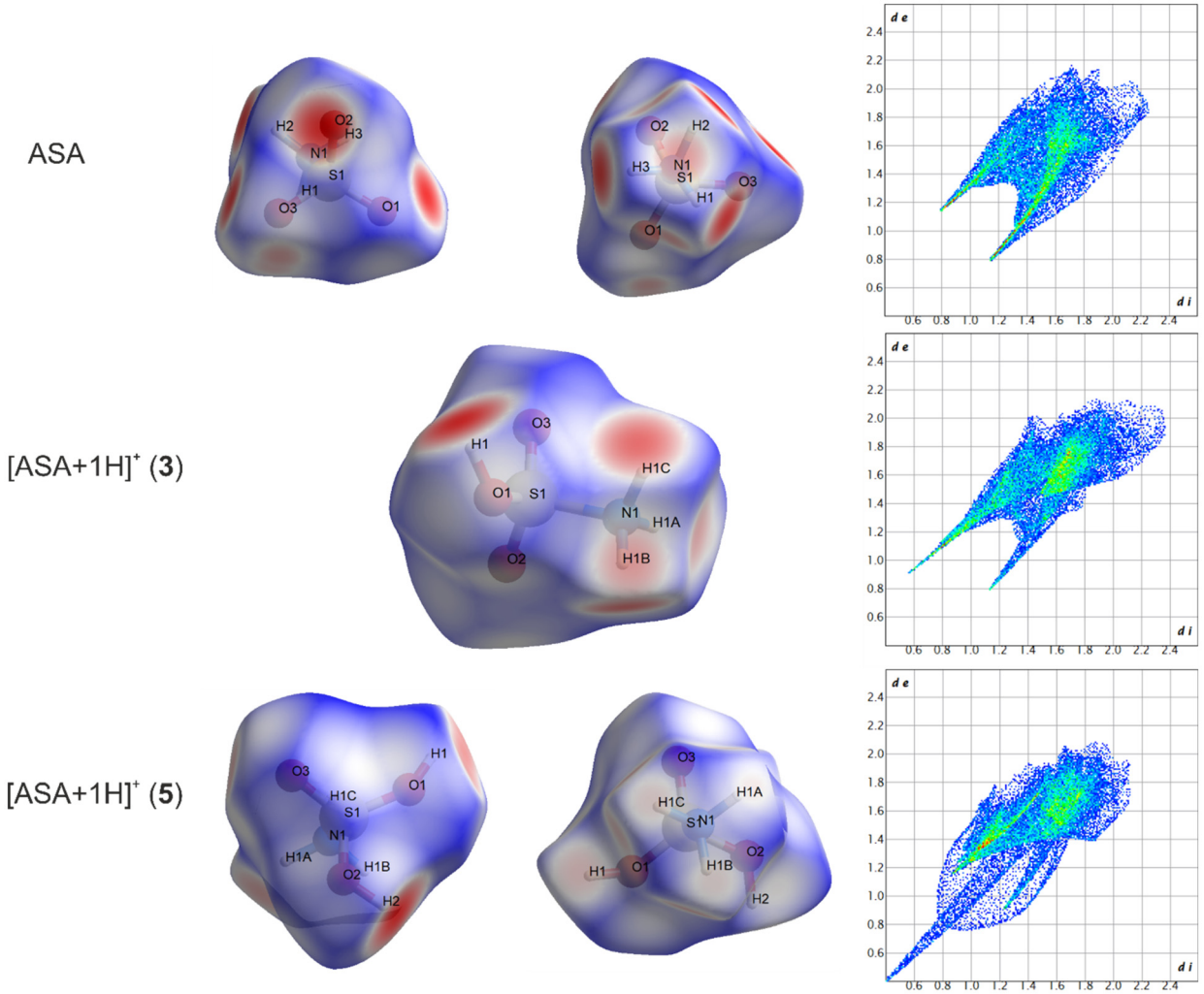

Fig. 9 Left: Two-dimensional fingerprint plots of the corresponding crystal structures of ASA and [ASA + 1H]$^+$ salts (**3** and **5**). Right: Distribution of the close contacts as a ring diagram and the corresponding Hirshfeld surfaces. (de: distance from the Hirshfeld surface to the nearest atom exterior; di: distance from the Hirshfeld surface to the nearest atom interior).

were carried out using Crystal17 with the DFT-TZVP/PBE0-(D3) method. For details see experimental part based on the solid state structures determined by X-ray diffraction. The MEPs were calculated together with natural population analysis charges (NPAs) to gain insight into the charge distribution of the zwitterionic character of ASA and its protonated species. In Fig. 11 and 12, the mapped electrostatic potentials (MEPs) of ASA and [ASA + 1H]$^+$ are shown. The SI lists the NPA charges and NBO charges of the shown compounds.

In the MEP of ASA the negative electrostatic potential (red) is located at the sulfonate oxygen atoms. The positive electrostatic potential (blue) can be located at the ammonium moiety.

In the MEP of [ASA + 1H]$^+$ the least positive electrostatic potentials (red) are located at the sulfuryl oxygen atoms of the sulfonic acid moiety. The positive electrostatic potential (blue) can be located at the ammonium moiety, as well as the acidic proton on the sulfonic acid moiety.

Experimental

General

Caution! The hydrolysis of BF_3, GeF_4, AsF_5, SbF_5 and the prepared salts (**2–5**) might form HF, which burns skin and causes irreparable damage. Safety precautions must be taken while using and handling these materials.

Apparatus and materials

The reactions were carried out according to Schlenk's standard procedure with a stainless-steel vacuum line. Fluorinated ethylene propylene (FEP)/per-fluoralkoxy (PFA) reactors sealed with a stainless-steel valve were used for all of the reactions in superacid media. Both the vacuum line and the reactors were dried with fluorine before use. Raman spectroscopic studies at low temperatures were performed using a Bruker MultiRAM FT-Raman spectrometer with Nd:YAG laser excitation (λ = 1064 cm^{-1}) under vacuum at −196 °C. For measurement, the

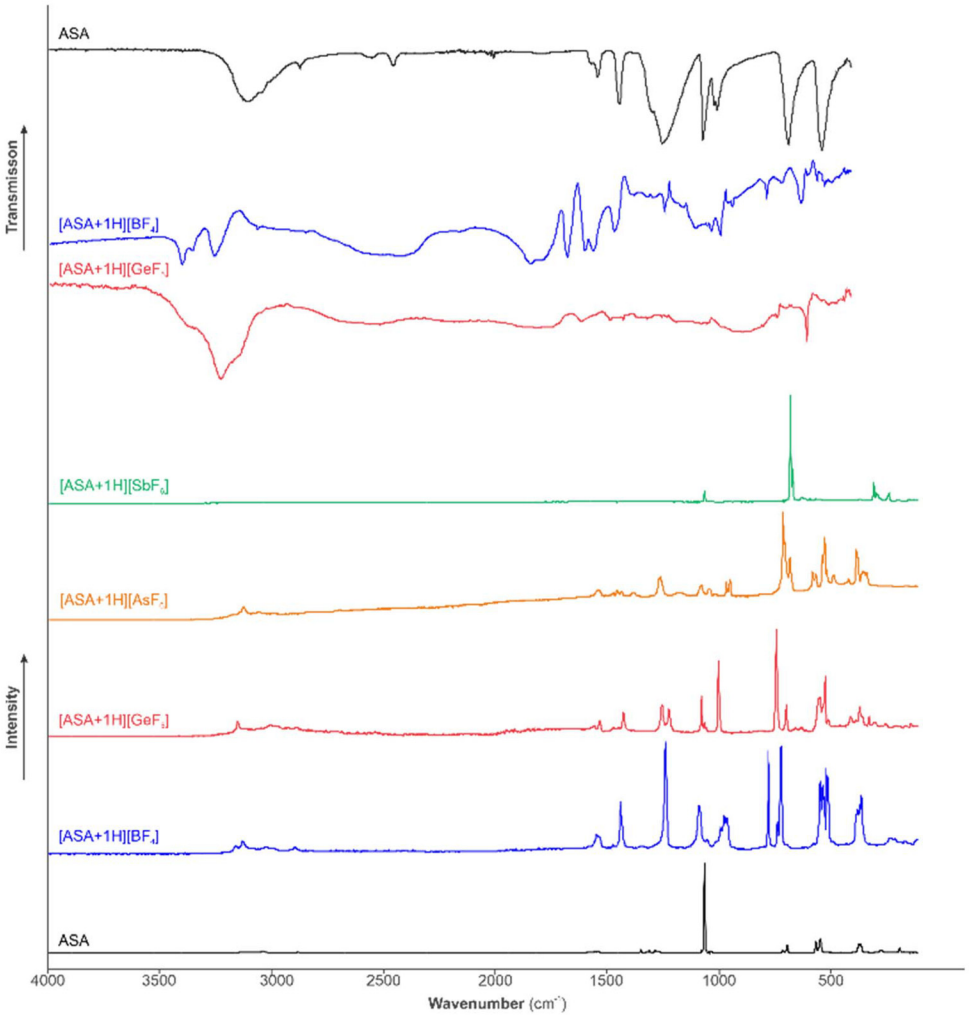

Fig. 10 Low-temperature IR (**1–3**) and Raman spectra of ASA and protonated species $[ASA + 1H]^+$ (**2–5**).

synthesized compounds were transferred into a cooled glass cell at low temperatures. IR spectra were recorded in a vacuum using a Bruker Vertex-80 VFTIR spectrometer. A small amount

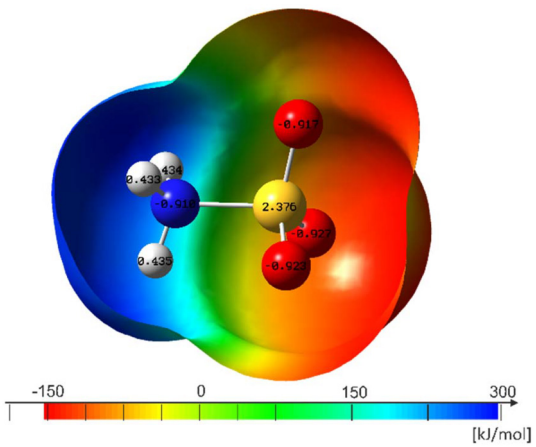

Fig. 11 Molecular 0.0004 $bohr^{-3}$ 3D isosurfaces with MEP on a color scale ranging from –152.3 kJ mol^{-1} (red) to 294.1 kJ mol^{-1} (blue). The electrostatic potential isosurfaces and the NPA charges have been calculated for ASA.

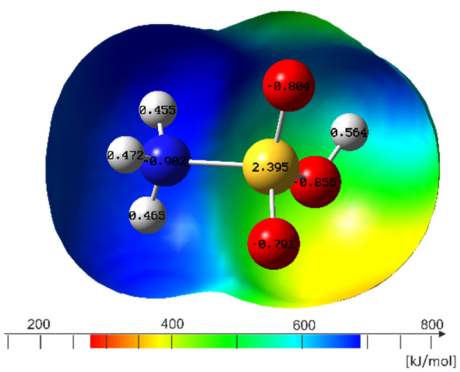

Fig. 12 Molecular 0.0004 $bohr^{-3}$ 3D isosurfaces with MEP on a color scale ranging from 275.7 kJ mol^{-1} (red) to 682.6 kJ mol^{-1} (blue). The electrostatic potential isosurfaces and the NPA charges have been calculated for ASA.

of the synthesized samples were placed on a CsBr single-crystal plate in a low-temperature cell for measurement.[27] Low-temperature single-crystal X-ray diffraction of ASA (**1**), [ASA + 1H][BF_4]·ASA (**2**), [ASA + 1H][GeF_5] (**3**), [ASA + 1H][AsF_6] (**4**) and [ASA + 1H][SbF_6] (**5**) was performed on an Oxford XCalibur 3 diffractometer equipped with a Kappa CCD detector, operating with MoKα (0.71073 Å) radiation and a Spellman generator (voltage 50 kV, current 40 mA). The program CrysAlisPro 1.171.38.46 (Rigaku OD, 2015) was employed for data collection and reduction.[28] The structures were solved utilizing SHELXT[29] and SHELXL-2018/3[30] of the WINGX software package.[31] The structures were checked using the software PLATON.[32] The absorption correction was performed using the SCALE3 ABPSACK multi-scan method.[33] Visualization was done with the software Mercury.[34] Selected data and parameters of the measured single-crystal X-ray structure analyses are summarized in Tables S1 and S2 (see SI). The quantum chemical calculations were performed at the MP2/aug-cc-pVTZ level of theory. For visualization and illustration of the MEP calculations, GaussView 6.0 was used.[35,36]

Periodic quantum-chemical calculations were carried out for all discussed compounds with the PBE0 hybrid density functional theory method (DFT-PBE0).[37,38] All calculations were performed with the CRYSTAL17 program package.[39] Triple-ζ-valence + polarization (TZVP) level basis sets were applied for C, O, S, N, H, F, B, Ge, Sb and As. The basis sets have been previously derived from the Karlsruhe def2 basis sets and can be found elsewhere in literature.[40–44] Intermolecular van der Waals dispersion interactions were taken into account using Grimme's empirical D3 dispersion correction with zero damping.[45] Reciprocal space was sampled by Monkhorst–Pack-type *k*-point grids: 6 × 3 × 2 for [ASA + 1H][GeF_5], 6 × 4 × 3 for [ASA + 1H][SbF_6], 4 × 4 × 3 for ASA, 6 × 4 × 3 for [ASA + 1H][AsF_6] and 3 × 6 × 2 for [ASA + 1H][BF_4]·ASA.[46] For the evaluation of the Coulomb and exchange integrals (TOLINTEG), tolerance factors of 8, 8, 8, 8, and 16 were used for ASA and [ASA + 1H][BF_4]·ASA, 6, 6, 6, 6 and 12 for [ASA + 1H][GeF_5], 7, 7, 7, 7, 14 for [ASA + 1H][SbF_6] and 8, 8, 8, 8, and 16 for [ASA + 1H][AsF_6]. Both the atomic positions and lattice parameters were fully optimized within the constraints imposed by the space group symmetry. Default DFT integration grids and optimization convergence thresholds were applied in all calculations. The harmonic vibrational frequencies and Raman and IR intensities were obtained through usage of the computational Scheme implemented in CRYSTAL17.[47–50] Raman and IR intensities were calculated for a polycrystalline powder sample (total isotropic intensity in arbitrary units). The Raman spectra were obtained by using a pseudo-Voigt band profile (50 : 50 Lorentzian : Gaussian) and a full width at half-maximum (fwhm) of 8 cm^{-1} and simulated considering the experimental setup (293.15 K; λ = 532 nm). Bands for the Raman and IR spectrum were assigned by visual inspection of the normal modes with the Jmol program package at https://crysplot.crystalsolutions.eu/.[51,52] To further explore the stabilization effects of the in the solid state, of ASA and protonated species **3** and **5**, a Hirshfeld surface analysis of the interionic contacts was conducted.[53]

[ASA + 1H][BF_4]·ASA (RT)

ASA (97.1 mg, 1.00 mmol, 1.0 eq.) was filled into an FEP reactor, aHF (50.0 mg, 2.50 mmol, 2.5 eq.) and BF_3 (136 mg, 2.00 mmol, 2.0 eq.) were condensed into the vessel. The reactants were warmed to room temperature and thoroughly mixed for 3 min. A colorless precipitant was formed. The excess solvent was removed *in vacuo* at −78 °C. The product [ASA + 1H][BF_4]·ASA was obtained as a colorless solid in quantitative yield.

[ASA + 1H][GeF_5] (RT)

ASA (97.1 mg, 1.00 mmol, 1.0 eq.) was filled into an FEP reactor, aHF (100 mg, 5.00 mmol, 5.0 eq.) and GeF_4 (594 mg, 4.00 mmol, 4.0 eq.) were condensed into the vessel. The reactants were warmed to room temperature and thoroughly mixed for 3 min. A colorless precipitate was formed. The excess solvent was removed *in vacuo* at −78 °C. The product [ASA + 1H][GeF_5] was obtained as a colorless solid in quantitative yield.

[ASA + 1H][AsF_6] (RT)

ASA (97.1 mg, 1.00 mmol, 1.0 eq.) was filled into an FEP reactor, *a*HF (60.03 mg, 3.0 mmol, 3.0 eq.) and AsF_5 (340 mg, 2.00 mmol, 2.0 eq.) were condensed into the vessel. The reactants were warmed to room temperature and thoroughly mixed for 3 min. A colorless precipitate was formed. The excess solvent was removed *in vacuo* at −78 °C. The product [ASA + 1H][AsF_6] was obtained as a colorless solid in quantitative yield.

[ASA + 1H][SbF_6] (RT)

SbF_5 (280 mg, 1.29 mmol, 2.0 eq.) was condensed into an FEP and dissolved in aHF (60.03 mg, 3.0 mmol, 3.0 eq.). ASA (62.6 mg, 0.645 mmol, 1.0 eq.) was filled into the vessel. The reactants were warmed to room temperature and thoroughly mixed for 3 min. A colorless precipitate was formed out of a turquoise solution. The excess solvent was removed *in vacuo* at −78 °C. The product [ASA + 1H][SbF_6] was obtained as a colorless solid in quantitative yield.

Conclusions

In the binary superacidic media HF/L (L = BF_3, AsF_5, SbF_5) ASA reacts under the formation of ammonium sulfonic acid salts $[H_3NSO_3H]^+[LF]^-$. Depending on the preferred coordination of the provided Lewis acid, mono- or twofold hemi protonated species are formed. The obtained monoprotonated salts were isolated and characterized by low-temperature vibrational spectroscopy, and single-crystal structure analyses and quantum chemical calculations DFT-TZVP/PBE0-(D3) method. The synthesized superelectrophile cannot be protonated further to achieve the formation of the ammonium sulfonium dication

$[H_3NSO_3H_2]^{2+}$, as the positive atomic charge of the sulfur would be 3+. Upon deprotonation of ASA no anionic species could be obtained which is in contrast to aminomethanesulfonic acid.

Conflicts of interest

There are no conflicts to declare.

Data availability

The data supporting this article have been included as part of the supplementary information (SI). Supplementary information: full details on vibrational spectroscopy, X-ray diffraction refinement, and computational details. See DOI: https://doi.org/10.1039/d5dt02262b.

CCDC 2418182 (ASA), 2418183 ([ASA + 1H][AsF_6]), 2418186 ([ASA + 1H][BF_4]·ASA), 2418188 ([ASA + 1H][GeF_5]), 2418190 ([ASA + 1H][SbF_6]) and 2418192 ($(NH_4)_2[Cu(H_2O)_6](SO_4)_2$) contain the supplementary crystallographic data for this paper.[54a–f]

Acknowledgements

Prof. Dr A. J. Kornath passed away unexpectedly in March 2024. We are grateful to the Department of Chemistry at the Ludwig Maximilian University of Munich, the Deutsche Forschungsgemeinschaft (DFG), the F-Select GmbH, and Prof. Dr. Karaghiosoff for their support.

References

1 A. Metzger, Sulfamic Acid, in *Ullmann's Encyclopedia of Industrial Chemistry*, Wiley-VCH, Weinheim, 2000.
2 L. B. Clapp, Sulfamic acid and its uses, *J. Chem. Educ.*, 1943, **20**(4), 189.
3 K. A. Hofmann, E. Bielsacki and E. Söderlund, *Ber. Dtsch. Chem. Ges.*, 1912, **45**, 1731.
4 R. Paetzolf, K. Dostal and A. RutICKA, *Z. Anorg., Allg. Chem.*, 1966, **348**, 1.
5 A. B. Burg, *J. Am. Chem. Soc.*, 1943, **65**, 322.
6 F. Beiat, e. Kratky, E. Nachbaur and A. Popitsch, *Mh. Chem.*, 1987, **118**, 947.
7 F. Watari, *Z. Anorg., Allg. Chem.*, 1964, **332**, 322.
8 R. L. Sass, *Acta Crystallogr.*, 1960, **13**(4), 320–324.
9 G. Albrecht and R. B. Corey, *J. Am. Chem. Soc.*, 1939, **61**(5), 1087–1103.
10 R. E. Khoma, V. O. Gel'mbol'dt, O. V. Shishkin, V. N. Baumer and L. V. Koroevaa, *Russ. J. Gen. Chem.*, 2013, **83**(5), 969–971.
11 J. P. Candlin and R. G. Wilkins, *J. Chem. Soc.*, 1960, 4236–4241.
12 M. Hopfinger, K. Lux, F. Schubert and A. Kornath, *Acta Crystallogr.*, 2011, **C67**, 400.
13 V. Bockmair, A. Klöck, D. Hollenwäger and A. J. Kornath, *Acta Crystallogr.*, 2024, **C80**, 401–406.
14 M. Hopfinger, *Protonierte Schwefelsäuren (Dissertation, Chemie und Pharmazie)*, LMU, München, 2012.
15 T. S. Cameron, C. K. Prout, F. J. C. Rossotti and D. Steele, Chemical Crystallography Laboratory, *J. Chem. Soc., Dalton Trans.*, 1972, 1590–1592.
16 B. N. Figgis, A. N. Sobolev, C. J. Simmons, M. A. Hitchman, H. Stratemeier and M. J. Riley, *Acta Crystallogr.*, 2000, **B56**, 438–443.
17 G. A. Jeffrey, *An introduction to hydrogen bonding; Topics in physical chemistry; Topics in physical chemistry*, Oxford Univ. Press, 1997.
18 T. Rennebaum, D. van Gerven, F. C. H. Herwede and M. S. Wickleder, *Chem. – Eur. J.*, 2024, **30**, e202402337, DOI: 10.1002/chem.202402337.
19 V. Bockmair, O. Ewert, J. Hofstädter, D. Hollenwäger and A. J. Kornath, *Inorg. Chem.*, 2025, **64**(39), 19545–19554, DOI: 10.1021/acs.inorgchem.5c01993.
20 M. C. Bayer, N. Greither, V. Bockmair, A. Nitzer and A. J. Kornath, *Eur. J. Inorg. Chem.*, 2022, **2022**, 1–8.
21 V. Bockmair, C. Hoch, I. Schusterbauer and A. J. Kornath, *Acta Crystallogr.*, 2024, **C80**, 1–6, DOI: 10.1107/S2053229624006338.
22 T. E. Mallouk, B. Desbat and N. Bartlett, *Inorg. Chem.*, 1984, **23**(20), 3160–3166.
23 C. Jessen and A. J. Kornath, *Eur. J. Inorg. Chem.*, 2022, **2022**, e202100965.
24 M. C. Bayer, C. Jessen and A. Kornath, *Z. Anorg. Allg. Chem.*, 2020, **646**, 333–339, DOI: 10.1002/zaac.202000091.
25 M. W. Wong, K. B. Wiberg and M. J. Frisch, *J. Am. Chem. Soc.*, 1992, **114**(2), 523–529.
26 V. Bockmair, T. Xu, D. Hollenwäger and A. J. Kornath, *Dalton Trans.*, 2025, **54**, 12169–12179, DOI: 10.1039/D5DT00864F.
27 L. Bayersdorfer, R. Minkwitz and J. Jander, *Z. Anorg. Allg. Chem.*, 1972, **392**(2), 137–142.
28 Rigaku Oxford Diffraction. *CrysAlisPro Software System; Version 1.171.39.46e*, 2018.
29 G. M. Sheldrick, SHELXT - integrated space-group and crystalstructure determination, *Acta Crystallogr.*, 2015, **71**(1), 3–8.
30 G. M. Sheldrick, Crystal structure refinement with SHELXL, *Acta Crystallogr.*, 2015, **71**(1), 3–8.
31 L. J. Farrugia, WinGX suite for small-molecule single-crystal crystallography, *J. Appl. Crystallogr.*, 1999, **32**(4), 837–838.
32 A. L. Spek, Single-crystal structure validation with the program PLATON, *J. Appl. Crystallogr.*, 2003, **36**(1), 7–13.
33 SCALE3 ABSPACK, an Oxford Diffraction Program; Oxford Diffraction Ltd, 2005.
34 C. F. Macrae, I. Sovago, S. J. Cottrell, P. T. A. Galek, P. McCabe, E. Pidcock, M. Platings, G. P. Shields, J. S. Stevens, M. Towler and P. A. Wood, Mercury 4.0: from

visualization to analysis,design and prediction, *J. Appl. Crystallogr.*, 2020, **53**(1), 226–235.

35 M. J. Frisch, G. W. Trucks, H. B. Schlegel, G. E. Scuseria, M. A. Robb, J. R. Cheeseman, G. Scalmani, V. Barone, B. Mennucci, G. A. Petersson, H. Nakatsuji, M. Caricato, X. Li, H. P. Hratchian, A. F. Izmaylov, J. Bloino, G. Zheng, J. L. Sonnenberg, M. Hada, M. Ehara, K. Toyota, R. Fukuda, J. Hasegawa, M. Ishida, T. Nakajima, Y. Honda, O. Kitao, H. Nakai, T. Vreven, J. A. Montgomery, J. E. Peralta, F. Ogliaro, M. Bearpark, J. J. Heyd, E. Brothers, K. N. Kudin, V. N. Staroverov, R. Kobayashi, J. Normand, K. Raghavachari, A. Rendell, J. C. Burant, S. S. Iyengar, J. Tomasi, M. Cossi, N. Rega, J. M. Millam, M. Klene, J. E. Klene, J. E. Know, J. B. Cross, V. Bakken, C. Adamo, J. Jaramillo, R. Gomperts, R. E. Stratmann, O. Yazyev, A. J. Austin, R. Cammi, C. Pomelli, J. O. Ochterski, R. L. Martin, K. Morokuma, V. G. Zakrzweski, G. A. Voth, P. Salvador, J. J. Dannenberg, S. Dapprich, A. D. Daniels, O. Farkas, J. B. Foresman, J. V. Ortiz, J. Cioslowski and D. J. Fox, *Gaussian16, Revision C.01*, Gaussian Inc., Wallingford CT, 2016.

36 D. Roy, A. Keith Todd and J. M. Millam, *GaussView Version 6*, 2019.

37 C. Adamo and V. Barone, *J. Chem. Phys.*, 1999, **110**, 6158.

38 J. P. Perdew, K. Burke and M. Ernzerhof, *Phys. Rev. Lett.*, 1996, **77**, 3865.

39 R. Dovesi, A. Erba, R. Orlando, C. M. Zicovich-Wilson, B. Civalleri, L. Maschio, M. Rérat, S. Casassa, J. Baima, S. Salustro and B. Kirtman, *Wiley Interdiscip. Rev.: Comput. Mol. Sci.*, 2018, **8**, e1360.

40 F. Weigend and R. Ahlrichs, *Phys. Chem. Chem. Phys.*, 2005, **7**, 3297.

41 A. J. Karttunen, T. Tynell and M. Karppinen, *J. Phys. Chem. C*, 2015, **119**, 13105.

42 T. Wylezich, R. Valois, M. Suta, A. Mutschke, C. Ritter, A. Meijerink, A. J. Karttunen and N. Kunkel, *Chem. – Eur. J*, 2020, **26**, 11742.

43 L. M. Scherf, A. J. Karttunen, O. Pecher, P. C. M. M. Magusin, C. P. Grey and T. F. Fässler, *Angew. Chem., Int. Ed.*, 2016, **55**, 1075.

44 B. Scheibe, A. J. Karttunen, F. Weigend and F. Kraus, *Chem. – Eur. J.*, 2021, **27**, 2381.

45 S. Grimme, J. Antony, S. Ehrlich and H. Krieg, *J. Chem. Phys.*, 2010, **132**, 154104.

46 H. J. Monkhorst and J. D. Pack, *Phys. Rev. B*, 1976, **13**, 5188.

47 C. M. Zicovich-Wilson, F. Pascale, C. Roetti, V. R. Saunders, R. Orlando and R. Dovesi, *J. Comput. Chem.*, 2004, **25**, 1873.

48 F. Pascale, C. M. Zicovich-Wilson, F. L. Gejo, B. Civalleri, R. Orlando and R. Dovesi, *J. Comput., Chem.*, 2004, **25**, 888.

49 L. Maschio, B. Kirtman, M. Rérat, R. Orlando and R. Dovesi, *J. Chem. Phys.*, 2013, **139**, 164102.

50 L. Maschio, B. Kirtman, R. Orlando and M. Rèrat, *J. Chem. Phys.*, 2012, **137**, 204113.

51 G. Beata, G. Perego, B. Civalleri and J. Comput, *Chem*, 2019, **40**, 2329.

52 Jmol: an open-source Java viewer for chemical structures in 3D. https://www.jmol.org/.

53 S. K. Wolff, D. J. Grimwood, J. J. McKinnon, M. J. Turner, D. Jayatilaka and M. A. Spackman, *CrystalExplorer 17.5, f4e298a*; University of Western Australia, Revision, 2017.

54 (*a*) CCDC 2418182: Experimental Crystal Structure Determination, 2025, DOI: 10.5517/ccdc.csd.cc2m59w0; (*b*) CCDC 2418183: Experimental Crystal Structure Determination, 2025, DOI: 10.5517/ccdc.csd.cc2m59x1; (*c*) CCDC 2418186: Experimental Crystal Structure Determination, 2025, DOI: 10.5517/ccdc.csd.cc2m5b05; (*d*) CCDC 2418188: Experimental Crystal Structure Determination, 2025, DOI: 10.5517/ccdc.csd.cc2m5b27; (*e*) CCDC 2418190: Experimental Crystal Structure Determination, 2025, DOI: 10.5517/ccdc.csd.cc2m5b49; (*f*) CCDC 2418192: Experimental Crystal Structure Determination, 2025, DOI: 10.5517/ccdc.csd.cc2m9l6r.